Quentin Frederick[a], Thomas Burks[a], Pappu Kumar Yadav[b], Jianwei Qin[c], Moon Kim[c], Megan Dewdney[d]

[a]Department of Agricultural and Biological Engineering, P.O. Box 110570, University of Florida, Gainesville, FL 32611-0570, USA; [b]Department of Agricultural and Biosystems Engineering, P.O. Box 2100, South Dakota State University, Brookings, SD 57007, USA; [c]USDA/ARS Environmental Microbial and Food Safety Laboratory, Beltsville Agricultural Research Center, Beltsville, MD 20705, USA; [d]Citrus Research and Education Center, 700 Experiment Station Rd. Lake Alfred, FL 33850, USA

Supervised Hyperspectral Band Selection using Texture Features for Classification of Citrus Leaf Diseases with YOLOv8

A paper from the Proceedings of the
16th International Conference on Precision Agriculture
21-24 July 2024
Manhattan, Kansas, United States

Abstract.

Citrus greening disease (HLB) and citrus canker are diseases afflicting Florida citrus groves, causing financial losses through smaller fruits, blemishes, premature fruit drop and/or eventual tree death. Often, symptoms of these resemble those of other defects or infections. Since HLB mitigation relies on prevention, early detection of HLB and canker via in-grove automated leaf inspection can enable more effective management of groves. Thus, vision-based in-grove disease scouting offers a financial benefit to the Florida citrus industry. This study tests methods of band selection from hyperspectral reflectance imagery (HSI) for classifying these two conditions in the presence of other, less consequential leaf defects. Hyperspectral reflectance images (400-1000 nm) of both sides of citrus leaves with visible symptoms of HLB, canker, zinc deficiency, scab, melanose, greasy spot, and a control class were collected with a line-scan HSI camera. Spectral bands from this imagery were selected using three methods: a random selection, Analysis of Variance (ANOVA) ranking of intensity values, and ANOVA with GLCM features. Using the selected bands, the YOLOv8 nano and small network architectures were trained to classify these images. The small network using an intensity-based band combination yielded an overall weighted F1 score of 0.8959, classifying HLB and canker with F1 scores of 0.788 and 0.941, respectively. This model variation also returned higher recall of canker (0.944) than any other model, despite a lower recall of HLB (0.941) than any other model. Confusion involving the control class was the primary error mode for most models. GLCM-based band

selection did not improve results, and the band combination appeared to exert less influence on the classification performance than the network size selected. These findings suggest that YOLOv8 relies more heavily on intensity differences than texture properties of citrus leaves, and is less sensitive to the choice of wavelengths than are traditional machine vision classifiers.

Keywords.
Hyperspectral, citrus, HLB, YOLO, GLCM, texture features, inspection, leaves, band selection, multiclass classification.

Introduction

The citrus industry contributes significantly to the economy of the state of Florida, which is currently the top domestic supplier for the U.S. orange juice market (Weber et al. 2024). Fruit production, juice production and marketing contributed approximately $6.9 billion to Florida's economy over the 2020-2021 season (Cruz, Court, and Ferreira 2023). In the 2022-2023 crop year, Florida produced 18.1 million boxes of citrus ("2022-2023 Citrus Summary" 2023). Although this sum is well short of the peak production of 300 million boxes per year recorded in the late 1990's, Florida supplied 28.6% of the USA's 2022-23 citrus production. Several factors, including hurricane damage, urban growth, a labor shortage, and the arrival of a few pathogens have all beset the Florida citrus industry recently. Citrus Greening Disease (HLB), a bacterial infection of Candidatus Liberibacter asiaticus and transmitted by the Asian citrus psyllid, was first recorded in Florida in 2005 (Bové 2006). Symptoms include mottling on leaves, twig dieback, and premature fruit drop. Also, fruit from infected trees is often of compromised quality (Dewdney, Vashisth, and Diepenbrock 2023). Currently, the best defenses against HLB are preventative, including removal of infected trees and psyllid control (Wang et al. 2017). Placing citrus groves underneath mesh screens to exclude psyllids (CUPS) is also being attempted (Schumann et al. 2023), but the long-term feasibility of this approach is not yet known.

Citrus canker is a bacterial infection caused by some strains of the Xanthomonas genus and has been present in Florida in varying levels of severity for over a century. Typically spread by wind and rain, this infection causes fruit drop and dieback (Gottwald, Graham, and Schubert 2002). An infected leaf or fruit will present raised lesions with a yellow halo surrounding them. Copper sprays can protect fruit from infection, but since leaves grow faster, copper is much less effective for protecting them (Dewdney and Johnson 2023). The state of Florida is a quarantined area for canker, requiring meeting additional regulations for shipping fruit out of the state ("Citrus Quarantine and Disease Detection Maps" 2024). In addition to these more dire infections, melanose, scab and greasy spot also can be found in Florida. These can be controlled with pesticides, and are not as costly as HLB and canker (Singerman and Arouca 2017). A difficulty of inspecting citrus groves is distinguishing HLB and canker from symptoms of more easily treatable conditions (H. Zhang et al. 2021). Citrus disease detection systems must distinguish diseased leaf surface from healthy, and perceive differences between infections.

Leaf Inspection

Neves et al. (2023) developed a low-cost, early detection system by testing several classifiers on features extracted from fluorescence imagery with a convolutional neural network (CNN) to distinguish canker, HLB, scab, and zinc deficiency. Kukreja et al. (2023) diagnosed canker severity on leaves using a CNN for feature extraction and support vector machines (SVM) for classification. Six different severities were classified with 94% accuracy. Pydipati et al. (2006) showed that scab and melanose can be more easily detected on the back side of citrus leaves due to higher contrast between the leaf surface and the lesions. Using RGB imagery and texture features, accuracies above 95% were measured with most models. In 2012, Cardinali et al. (2012) demonstrated that spectral differences allow HLB-infected leaves to be accurately distinguished from healthy leaves.

Hyperspectral Imagery & Band Selection

Instead of the three broad wavelength bands produced by RGB cameras, hyperspectral imagery (HSI) includes dozens or hundreds of images in narrow bands, which can facilitate detection by accentuating defects. It has been shown that analysis of HSI benefits from consideration of both spatial and spectral features (L. Zhang et al. 2018). Food inspection with HSI has proven successful commercially ("Case History: Hyperspectral Sorting Detects More" 2021; Tormala and Calbucci 2023). Defects detected with HSI include degradation of spinach leaves (Diezma

et al. 2013) and foreign objects in dried seaweed (Kwak et al. 2021). Fresh fruits inspected with HSI include nectarines (Huang et al. 2021), peaches (Liu et al. 2020), jujubes (Thien Pham and Liou 2022), pomegranates (Okere et al. 2023), and mangoes (Velásquez et al. 2024). As hyperspectral cameras become more compact and inexpensive (Hogan 2021; Duarte et al. 2022), in-field applications will become more widespread.

It is often desirable to reduce the number of hyperspectral bands before processing to reduce computational costs and avoid processing redundant information (Yang, Lee, and Gader 2014). This has been done with genetic algorithms (Yuan et al. 2020), orthogonal subspace projection (Shuaibu et al. 2018), sparse linear discriminant analysis (LDA) (J. Li and Qian 2011), entropy distance (Deng et al. 2019), and manual techniques (Wetterich et al. 2016). Alternatively, it is often desirable to select bands from the dataset, since extracted bands are less interpretable (Du and Yang 2008), and because once selected wavelengths are identified, a comparatively inexpensive multispectral camera can be used to capture future imagery at those wavelengths. Both the cost of the imaging hardware, and the cost of the image processing hardware must be considered on the way towards in-field early disease detection systems. Frederick et al. (2023) evaluated an unsupervised and a supervised HSI band selection method on a dataset of images of orange peels belonging to five classes. 1-5 bands were selected with each method and used to train a custom CNN. A peak overall accuracy of 94.9% was recorded for a model using SVM to classify five unsupervised bands. However, with fewer than two bands, the supervised bands yielded better classification with either classifier.

Gray Level Co-occurrence (GLCM) is a well-known, widely used texture feature extraction method (Rogers et al. 2023) based on relative frequency distributions (Haralick, Shanmugam, and Dinstein 1973). It has been applied to inspect crops and fresh produce, including bananas (Olaniyi et al. 2017), pomegranates (Gurubelli, Malmathanraj, and Palanisamy 2020) and grape leaves (Yogeshwari and Thailambal 2023). Likewise, bands from imagery of tomatoes (Cho et al. 2013) and orchard trees (Abbasi et al. 2020) have been selected with analysis of variance (ANOVA). Gómez-Flores et al. (2019) used GLCM features for multiclass citrus leaf disease inspection, reaching 81% accuracy. By testing separability of class means in each feature, ANOVA can be employed to 'score' each feature independently of all the others.

Deep Learning

Deep Learning (DL), specifically with the You Only Look Once (YOLO) series of networks, is an increasingly popular technique for remote sensing with HSI, offering the advantage of spectral and spatial feature extraction (S. Li et al. 2019). Nguyen et al. (2021) employed a CNN feature extractor to classify diseased grape vines with HSI, recording a peak accuracy of 75%. Modifications to YOLOv8's architecture and loss function have been studied for detection of maize and rice leaf infections (R. Li et al. 2024; Trinh et al. 2024). Although more often used for object detection, the YOLO series of CNNs can also classify entire images. Islam et al. (2023) trained YOLOv5, YOLOv7, and YOLOv8 to classify seven leafy vegetable diseases, with the last of these reaching 100% accuracy. Versions of the YOLOv8 architecture have been shown to be effective at citrus detection in the presence of several other disease classes. YOLOv4 has been trained (using a 2684-image dataset) to detect anthracnose, bacterial brown spot, and melanose on citrus leaves, and was recognized for detection speed (Dananjayan et al. 2022). Lyu et al. (2023) employed several variations of YOLOv5 to detect Asian citrus psyllids in outdoor images. Qiu et al. (2022) developed and tested YOLOv5 on RGB datasets of citrus leaves and fruit with both HLB and similar symptoms, with a peak F1 score of 85%.

YOLOv8 was released in 2023 (Solawetz and Francesco 2023), but has already been employed for citrus inspection. Lu et al. (2023) tested YOLOv8 to inspect citrus peels, finding that despite having the fewest parameters of all models tested, it was the second-best performing model. A variation of YOLOv8 was trained on RGB imagery of citrus leaves and fruits to detect and classify six different surface defects, including melanose, scab, and canker. Segmented defects were classified with 93% accuracy and 93% mAP (2023). However, this study used a dataset of over 3000 RGB images.

Both intensity- and texture-based features have contributed to plant inspection (Ngugi, Abelwahab, and Abo-Zahhad 2021). Despite CNNs' proven performance with RGB imagery, little work has combined HSI with YOLOv8 for citrus diseases. Previous work has indicated that supervised band selection improved classification (Frederick et al. 2024), but did not answer whether the major error modes were limitations of the dataset, the classifier, or the bands selected. Nor have previous studies considered spatial relationships when selecting bands for leaf inspection, despite CNNs' suitability for leaf inspection with texture features (Barburiceanu et al. 2021). This study demonstrates multiclass classification of diseased citrus leaves with multiple variants of the YOLOv8 architecture using hyperspectral imagery, and tests the effect of involving texture in band selection.

Objectives

The objectives of this study are to:

- Train YOLOv8 to classify citrus leaf images of seven disease classes (HLB, canker, zinc deficiency, scab, melanose, greasy spot, and control) composed of bands selected with three methods: ANOVA ranking of pixel values, ANOVA ranking of GLCM features, and random choice.
- Compare the overall and class-specific classification results of these trained models.
- Evaluate the sensitivity of the classification model to the choice of wavelengths selected and size of the classifier network.

Materials & Methods

Data Collection

Approximately 750 citrus leaves primarily from Valencia orange trees and bearing symptoms of scab, melanose, HLB, canker, greasy spot, zinc deficiency and a control class were sampled at the Citrus Research & Education Center (CREC) (Lake Alfred, FL). Leaves with only one condition were gathered—those with symptoms of multiple infections were excluded. These leaves were refrigerated and imaged within 48 hours of collection. 4-16 leaves from the same class were imaged at a time, depending on leaf size. Both the adaxial and abaxial sides were imaged.

The HSI system (Figure 1) was developed recently at the USDA ARS EMFSL, and provides imaging of 348 spectral bands in a wavelength range of 395-1005 nm. Samples were illuminated by two separate LED line lights (Metaphase Technologies, Bristol, PA, USA), which emit visible and near-infrared (VNIR) broadband light for reflectance imaging and ultraviolet-A (UV-A) excitation light for fluorescence imaging. The VNIR light employs LEDs at seven wavelengths, namely 428, 650, 810, 850, 890, 910, and 940 nm, while the UV-A light uses a single wavelength at 365 nm. The intensities of the LEDs at the eight wavelengths can be adjusted through two digital dimming controllers, with three channels each. Specifically, four channels are used to regulate the intensities at 365, 428, 650 nm, and a bundle of five NIR wavelengths (810, 850, 890, 910, and 940 nm). The lights are angled at approximately 6° from the vertical position to overlap their line illuminations on the sample surface. Reflectance and fluorescence signals in the VNIR range are collected using a miniature line-scan hyperspectral camera (Nano-Hyperspec VNIR, Headwall Photonics, Bolton, MA, USA), which integrates an imaging spectrograph and a CMOS focal plane array detector (12-bit and 1936×1216 pixels). To capture a wide-angle view, a lens is attached with a 5 mm focal length (Edmund Optics, Barrington, NJ, USA) to the camera. Finally, a long-pass gelatin filter (>400 nm, Kodak, Rochester, NY, USA) is attached to the lens to remove second-order effects from the UV-A excitation.

A reflectance standard panel, measuring 254×32×15 mm3 (Labsphere of North Sutton, NH, USA) is mounted alongside the black, thermoplastic sample holder (measuring 254×197×15 mm) to allow flat-field correction of the reflectance images. For line-scan image acquisition, a

linear motorized stage (FUYU Technology of Chengdu, Sichuan, China) moves the sample holder and the reflectance panel beneath the hyperspectral camera. The camera has a spatial resolution of 0.33 mm/pixel when set at a lens-to-sample distance of 285 mm. Each camera frame is scanned and an 810×348 (spatial × spectral) pixel region of interest (ROI) is extracted, covering a spectral range of 395–1005 nm. To prevent the influence of ambient light on the images, the LED lights, camera, reflectance panel, and sample tray are all housed in an aluminum composite enclosure. This HSI system, measuring 56 × 45 × 60 cm, is easily transportable, making it ideal for on-site and field experiments.

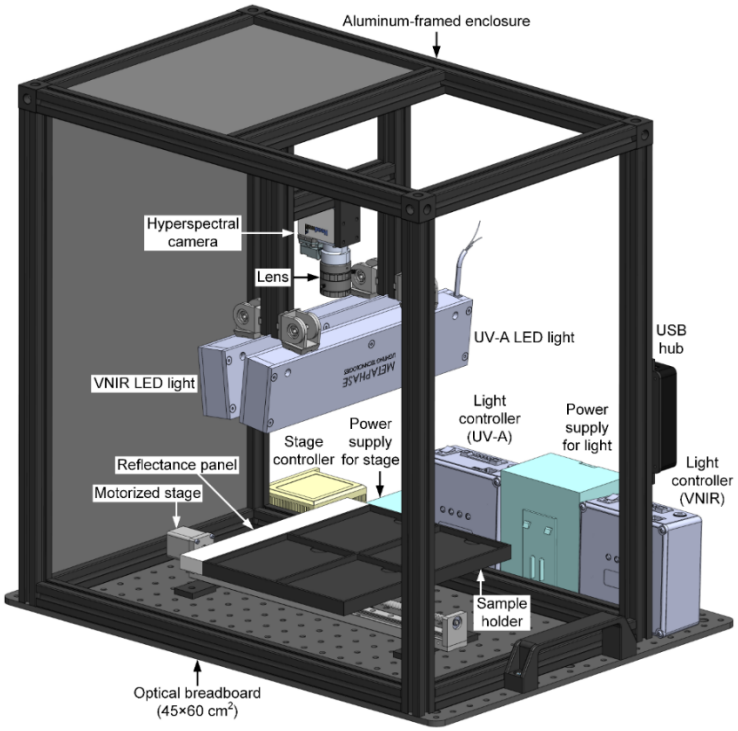

Fig. 1. A CAD rendering of the portable HSI system developed at USDA ARS EMFSL used to image leaves for this study

The system software for this HSI system was developed using LabVIEW (v2022, National Instruments, Austin, TX, USA) that runs on a Windows 11 (Microsoft Corporation, Redmond, Washington, U.S.A.) computer. A graphic user interface for the software was developed (Fig. 3) using LabVIEW's Vision Development Module (VDM) to enable image and spectrum display. To implement parameterization and data transfer functions, software development kits (SDKs) from hardware manufacturers were used, including User Datagram Protocol (UDP) for LED light control, Universal Serial Bus (USB) for camera control, and serial communication for stage movement control. The hyperspectral camera continuously collects line-scan reflectance signals as the sample holder is translated below it by a motorized stage. After each measurement, both the reflectance and fluorescence images acquired from the same samples are saved into two separate data files using a standard format of band interleaved by line (BIL). However, only hyperspectral reflectance images were used in this study.

Preprocessing

The raw reflectance values were converted to reflectance percentages with spectral calibration. This process also involved spectral and spatial binning, leaving a resolution of 1mm per pixel and 116 spectral bands. Next, a mask for each leaf was created by thresholding the saturation channel of the pseudocolor image and used to set the background pixel values to zero. This mask also facilitated spatial division of the images to leave a single leaf in each. Due to illumination irregularities, the first and last eight bands were removed from the dataset, as were images containing artifacts from camera overheating. The images of the front and back sides of each leaf in the dataset were then concatenated. Figure 2 displays a sample pseudocolor image from each class after preprocessing.

Fig. 2. A pseudocolor sample leaf image from each class after preprocessing

Band Selection

To test the effects of texture features, two 'feature matrices' were extracted for band selection. The first of these was composed of the image pixels, reshaped into a 2D matrix with rows corresponding to pixels and columns corresponding to features. The second feature matrix was formed by extracting five gray-level co-occurrence matrix (GLCM) texture features *from each band* and appending as a row. The GLCM quantifies occurrences of pairs of pixels values in an image, and is a well-known means of extracting texture features from imagery. Several statistical features can be extracted from the GLCM, and five were selected for this study: Contrast, Dissimilarity, Homogeneity, Correlation, and Angular Second Moment (ASM). Formulae for these features can be found in Gómez-Flores et al. (2019). Thus, each row of this second feature matrix corresponds to a HSI image and each column to a feature from a specific band. Both feature matrices were standardized.

For feature selection, Analysis of Variance (ANOVA) evaluates whether the difference between the means of different classes in each feature is significant using the F-statistic, thus quantifying the separability of the classes if that feature is retained. In this application, the features are wavelengths or texture features from wavelengths. Typically, only features whose F-statistic exceeds a selected significance level would be selected. However, exactly three bands were needed regardless of how many bands were significant, and adjacent bands are expected to contain much redundant information. Thus, bands were selected from both feature matrices' F-scores by lowering the local maxima neighborhood argument until at least three were selected, and using the three with the highest scores. The bands chosen using the GLCM feature matrix are referred to as GLCM bands, and those from the pixel intensity matrix as pixel bands. Also, to provide a baseline for the performance of each class, 20 random combinations of three bands were selected, and a model trained on each. Figure 3 summarizes the band selection procedures:

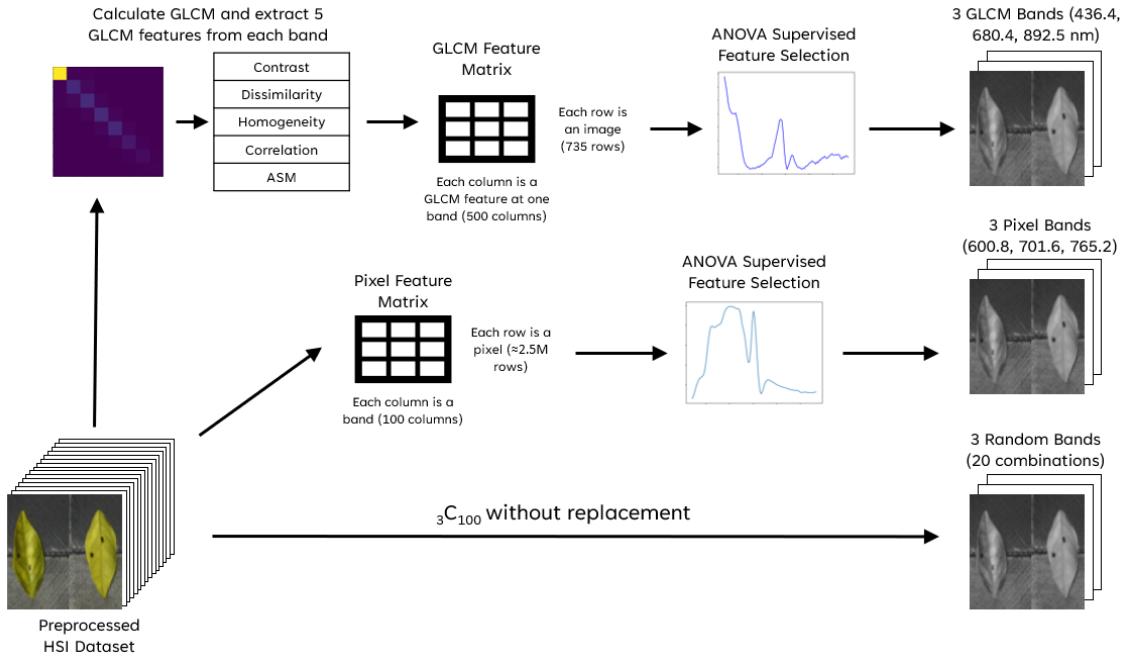

Fig 3. Summary of band selection methods

Network & Training Parameters

The 'nano' and 'small' versions of the YOLOv8 architecture (Jocher, Chaurasia, and Qiu [2022] 2023) were utilized, with a model of each size trained on each ANOVA band combination. The dataset was randomly split according to a 70/15/15 ratio of training, validation, and test data.

For ANOVA-based band selection, model hyperparameters were tuned using mutation-based hyperparameter tuning, for 50 iterations and 25 epochs per iteration. Default hyperparameters were used, except for 'flipud', 'degrees', 'shear', and 'perspective', which were initially set to 0.5, 1.0, 0.1, and 0.1, respectively, and object detection parameters 'mixup' and 'copy/paste', which were set to 0. For the random band combinations, default hyperparameters were used. Each model was trained for 300 epochs, with patience set to 50 epochs. The previously extracted feature matrices were used only for band selection and were not involved in model training.

Performance Evaluation

Overall model accuracy, precision, recall, and F1 score for each class were employed as performance metrics. For this application, recall is more critical than precision, especially for HLB and canker, since a false indication of one of these infections is less consequential than not detecting the infection. Table 1 states the formulae for these metrics, in terms of false positives (FP), true positives (TP), false negatives (FN), and true negatives (TN).

Table 1: Metrics employed to gauge classifier network performance.

Metric	Accuracy	Precision	Recall	F1 Score
Expression in terms of TP, FP, TN, and FN	$\frac{TP+TN}{TP+FP+TN+FN}$	$\frac{TP}{TP+FP}$	$\frac{TP}{TP+FN}$	$\frac{2TP}{2TP+FP+FN}$

Results & Discussion

Band Selection

The ANOVA F-statistics of the ASM features were all considerably higher than those of any of the other four GLCM features. Since the scoring of bands was univariate, no adjustment was made to the selection procedure and the three bands corresponding to the local maxima of the F-statistic curve were selected. These wavelengths were 441.7, 680.4, and 897.8 nm, and are

displayed with the F-statistics in Figure 4.

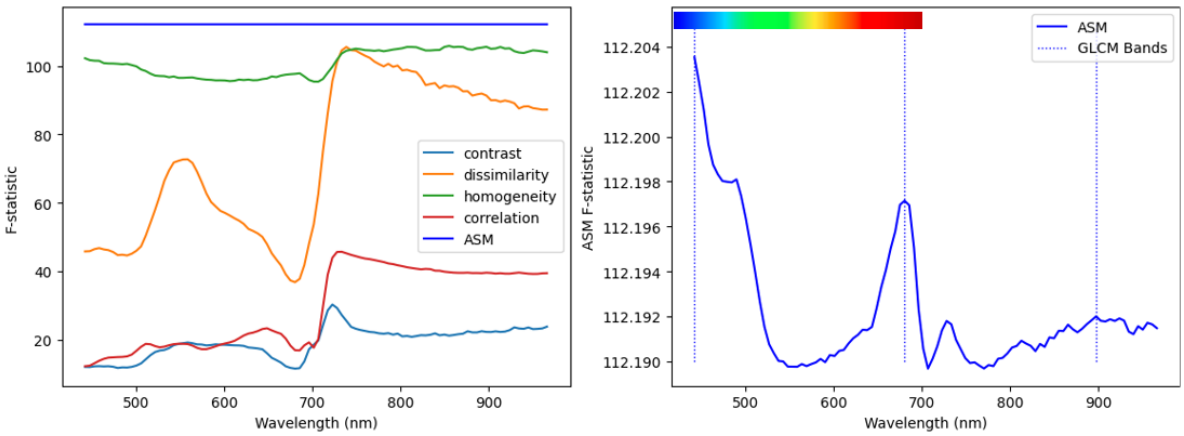

Fig. 4. GLCM feature matrix F-statistics and GLCM bands selected

The pixel feature matrix yielded wavelengths of 600.8, 701.6, and 765.2 nm, and the F-statistics for the pixel feature matrix are plotted in Figure 5 with the pixel bands.

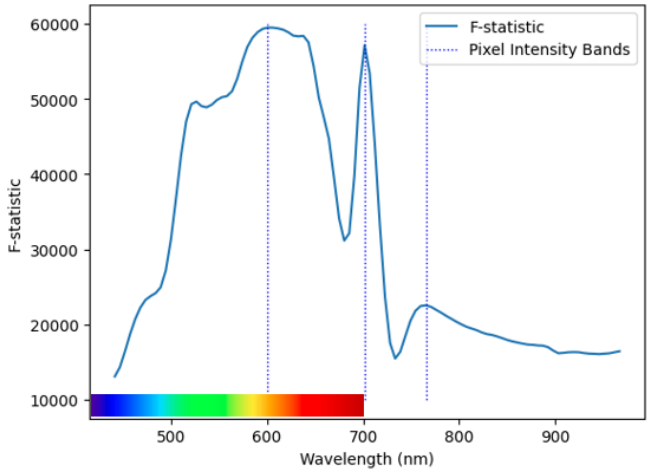

Fig. 5. Pixel-based F-statistics and resulting bands

Previous band selection work on this dataset also selected the 441.7 and 600.8 nm bands, but did not select any band above 722.8 nm. Supervised bands maximizing separability ranged from 489.5 to 600.8 nm (Frederick et al. 2024). This departure from the green range of the spectrum, especially for the pixel bands, is a result of using local extrema to counteract selection of adjacent bands—the range of previously selected bands all have F-statistics greater than 45000. Separability indicated by the peak at 765.2 nm was apparently not recognized by the previous methods.

Classification

Table 2 summarizes the overall performance of each model, including the mean accuracy and weighted F1 Score. Figures 6-8 display the percentage of images from each test set class that were classified into each class for all five models.

Table 2. Overall performance of all models. For the random band results, means and standard deviations are reported.

Band Selection Method	Wavelengths (nm)	Model Size	Accuracy (%)	Weighted F1 Score
GLCM	436.4, 680.4, 892.5	Nano	81.36	0.8156
		Small	88.13	0.8822
Pixels	600.8, 701.6, 765.2	Nano	86.44	0.8622
		Small	88.98	0.8959
Random Band Combinations		Nano	84.19 (σ = 4.3%)	0.8406 (σ = 0.044)

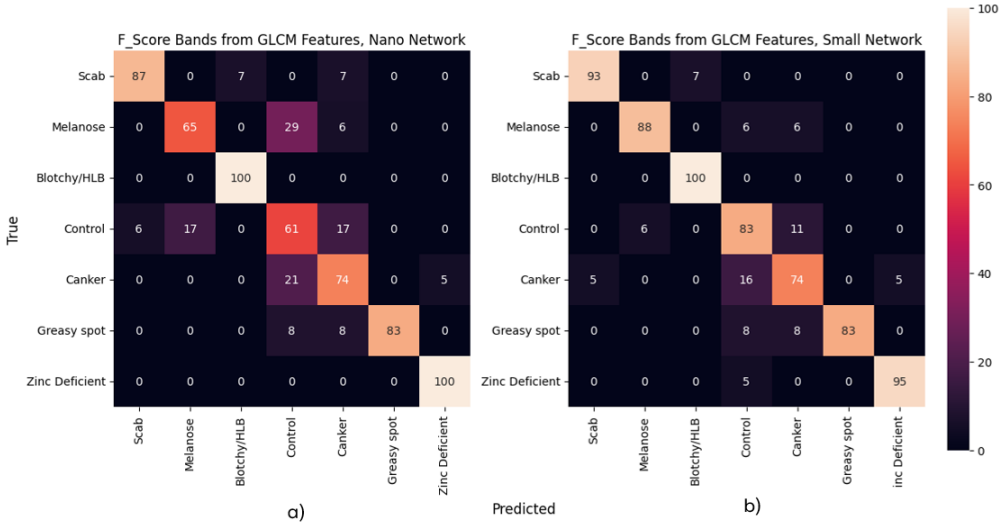

Fig. 6. Confusion matrices of classification models using GLCM features reported in percent of true samples

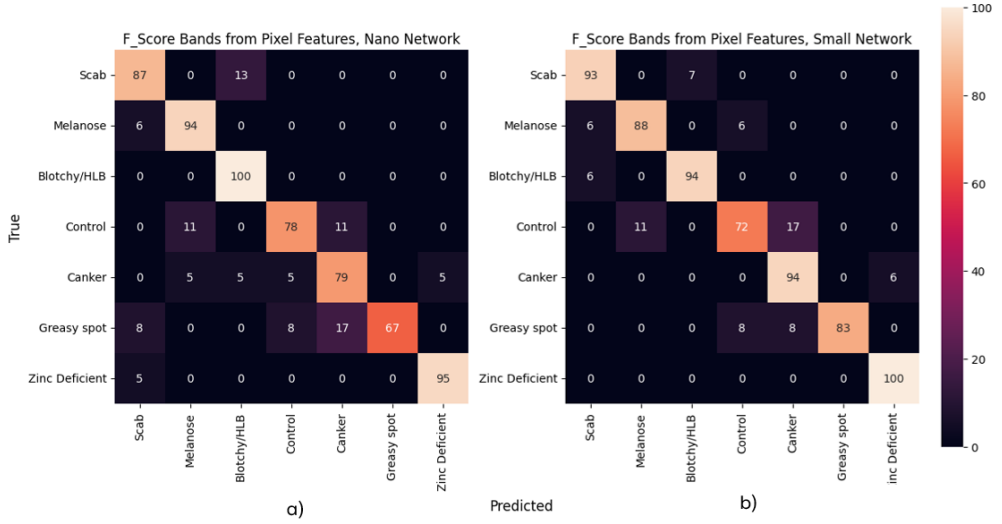

Fig. 7. Confusion matrices of classification models using Pixel (intensity) features reported in percent of true samples

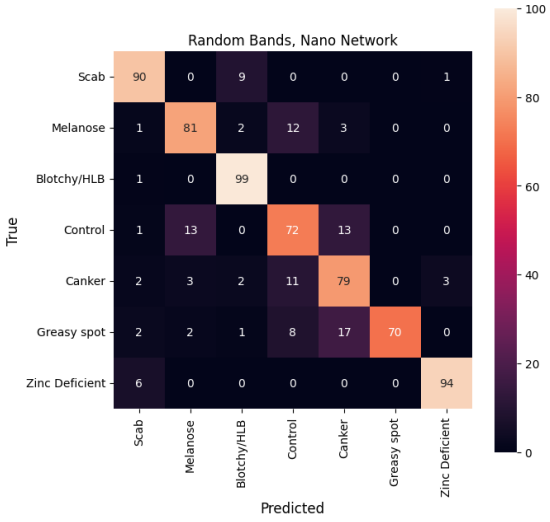

Fig. 8. Mean confusion matrices of classification models using three random bands reported in percent of true samples

Figures 9-10 display the class-specific results for each model. Distance from the center of the plots indicates higher values—for instance, for precision in Greasy Spot, the lines for each model lie at the edge of the plot. These metrics are also listed in Table 3. Overall performance

differences primarily stem from the Control, Canker, Melanose, and Greasy Spot classes.

Table 3. Precision, recall, and F1 scores for each class and each model.

		Control	Scab	Greasy Spot	Melanose	Canker	Zinc Deficient	Blotchy /HLB
Precision	Pixels, nano	0.875	0.813	1.000	0.842	0.789	0.950	0.850
	GLCM, nano	0.524	0.929	1.000	0.786	0.700	0.952	0.944
	GLCM, small	0.714	0.933	1.000	0.938	0.778	0.950	0.944
	Pixels, small	0.867	0.875	1.000	0.882	0.810	0.952	0.941
	Random Bands	0.736	0.857	0.989	0.816	0.762	0.961	0.886
Recall	Pixels, nano	0.778	0.867	0.667	0.941	0.789	0.950	1.000
	GLCM, nano	0.611	0.867	0.833	0.647	0.737	1.000	1.000
	GLCM, small	0.833	0.933	0.833	0.882	0.737	0.950	1.000
	Pixels, small	0.722	0.933	0.833	0.882	0.944	1.000	0.941
	Random Bands	0.725	0.897	0.700	0.815	0.792	0.935	0.991
F1 Score	Pixels, nano	0.839	0.800	0.889	0.789	0.824	0.950	0.919
	GLCM, nano	0.897	0.909	0.710	0.718	0.564	0.976	0.971
	GLCM, small	0.933	0.909	0.909	0.757	0.769	0.950	0.971
	Pixels, small	0.903	0.909	0.882	0.872	0.788	0.976	0.941
	Random Bands	0.873	0.816	0.811	0.771	0.726	0.947	0.934

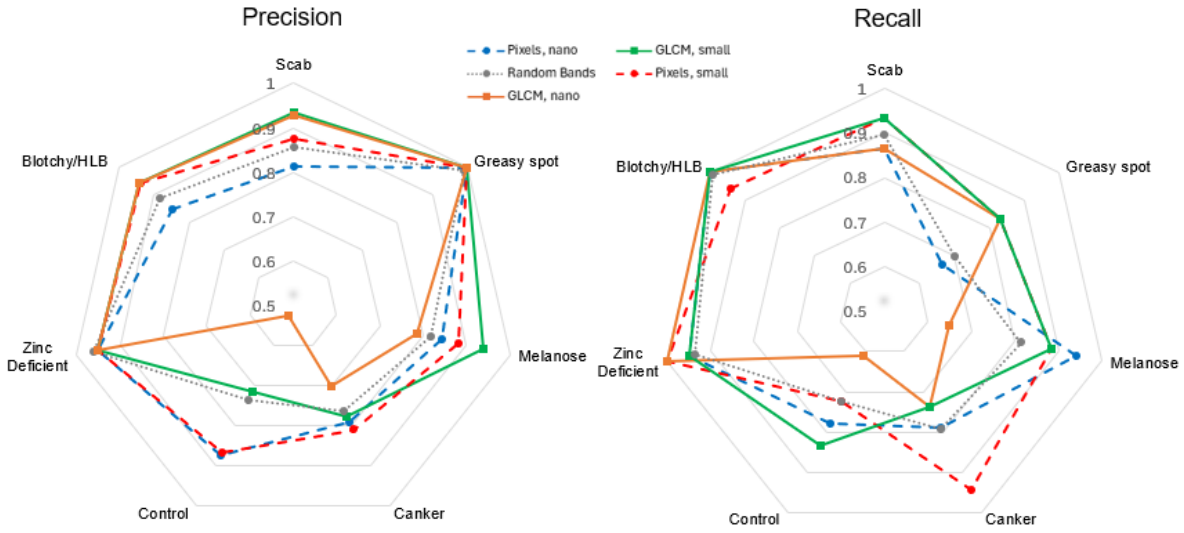

Fig. 9. Precision and Recall of all models with results for the random bands as means of all 20 models

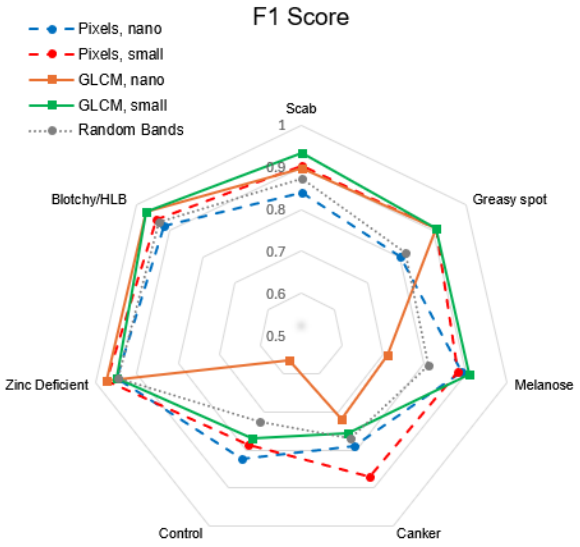

Fig. 10. F1 Scores of all models with mean results for the random band combinations.

Discussion

Of all the factors tested, network size exerts the greatest effect on classification performance. Each of the small models exceeded an 0.88 F1 score, whereas performance with the nano architecture varied between 0.82 and 0.86. The greatest difference between the highest performing model (pixel bands with a small network) and the others is observed in recall of Canker and Greasy Spot. Only for Greasy Spot did the GLCM bands show any clear advantage in recall. For small models, the GLCM bands displayed slightly improved recall in HLB, Scab, and Melanose, but considerably worse recall of Canker. The nano model using GLCM bands was outperformed in Control, Canker, and Melanose by both other nano models.

Recall of HLB was nearly equal for all models, as was precision of Greasy Spot. This can probably be attributed to HLB covering the majority of the leaf surface, while Greasy Spot and Melanose have very distinct discoloration regions, making them less likely to be hidden by the 1mm/pixel resolution. Zinc Deficient leaves, despite displaying a similar color to HLB, are generally smaller and leave more pronounced and visible leaf veins compared to HLB (see Fig. 2). As a result, this class was the best classified by all models.

For each model, the Control class created a major error mode, being misclassified into Melanose and Canker. Since practically all the leaves in the dataset will contain at least some healthy leaf area, classes whose symptoms are small lesions are particularly likely to be confused with Control. With the GLCM bands, Canker was also often mistaken for Control, but with the pixel bands, the Canker leaves were not misclassified into Melanose or Control.

Even without the benefit of hyperparameter tuning, the random band combinations generally matched the performance of the nano model using pixel bands. Only for Control and Melanose did the nano model with pixel bands substantially outperform the mean random model. This finding, paired with the standard deviation of the random band results, calls into question the necessity of intentional band selection for YOLOv8 classification to detect Canker and HLB. However, YOLO is limited to three bands, so band selection is still necessary. As can be seen in Figure 5, several bands surrounding 600 nm presented similar F-statistics. It is likely that these bands contain similar information and that combinations including any of them in place of 600.8 nm would yield similar performance. Similarly, compared to those of the other GLCM features, the range of the F-scores of the ASM features (<1) is very small relative to the values (≈112). This indicates that despite the classes being more separable with this GLCM feature than with any other, no band offers a substantial advantage for classification using ASM from that band.

Conclusion

Management of citrus pathogens requires distinguishing HLB and canker from other citrus leaf conditions. Hyperspectral imaging combined with deep-learning-based analysis permits accurate classification of these infections. Two supervised band selection methods were employed to select three wavelengths from hyperspectral imagery of both sides of citrus leaves. YOLOv8 was trained to classify these images, reaching an accuracy of 89.0% with a small YOLOv8 network and pixel intensity-based bands. With all band combinations, Zinc Deficiency and HLB were the best distinguished classes. Both ANOVA-based band combinations classified HLB with recall and F1 score of at least 0.941 and 0.919, respectively. Confusion between Canker and Control lowered the texture-based band combination's overall accuracies to 81.36% and 88.13% for the nano and small networks, respectively. Thus, these results fail to demonstrate that involving texture in the band selection process offers any performance improvement. A larger network significantly improves performance, but this benefit must be weighed against memory and processing requirements and suitability for in-field, embedded applications.

Future Work

A limitation of the classification approach is that each leaf can only be assigned to one disease

class. This is undesirable, since citrus diseases differ in frequency of occurrence and severity. Training a model for semantic segmentation of leaves into disease and healthy regions would permit detection of different infections on the same leaf, and avoid the possibility of false negatives in more critical pathogens.

Since ASM was shown to yield the highest F-statistics, no other GLCM features influenced band selection. However, it is not apparent whether and/or to what extent ASM corresponds to the textural features the classifier networks learned to exploit. Bands favored by the other textural features may complement YOLOv8 better. On a similar note, most models accurately identified HLB and Zinc deficiency, but confused Control, Canker, and Melanose. The band selection methods tested in this study treat all classes equally, despite two being the primary focus. Bands could be chosen to target major classification error modes. Although the mean results of the 20 random combinations of three bands were only slightly worse than the other nano models, they don't rule out a subset of wavelengths permitting significantly better classification than the others. It is possible that the mean performance results from a mixture of 'better' and 'worse' band choices. Further work might empirically identify this subset.

Acknowledgments

The authors would like to thank the CREC for hosting the data collection phase of this study and providing samples. The authors also gratefully acknowledge the financial support of USDA ARS Cooperative Agreement 58-8042-1-023.

References

"2022-2023 Citrus Summary." 2023. Maitland, FL: USDA National Agricultural Statistics Service. https://www.nass.usda.gov/Statistics_by_State/Florida/Publications/Citrus/Citrus_Summary/Citrus_Summary_Prelim/cit083123.pdf.

Abbasi, Mozhgan, Jochem Verrelst, Mohsen Mirzaei, Safar Marofi, and Hamid Reza Riyahi Bakhtiari. 2020. "Optimal Spectral Wavelengths for Discriminating Orchard Species Using Multivariate Statistical Techniques." *Remote Sensing* 12 (1): 63. https://doi.org/10.3390/rs12010063.

Barburiceanu, Stefania, Serban Meza, Bogdan Orza, Raul Malutan, and Romulus Terebes. 2021. "Convolutional Neural Networks for Texture Feature Extraction. Applications to Leaf Disease Classification in Precision Agriculture." *IEEE Access* 9:160085–103. https://doi.org/10.1109/ACCESS.2021.3131002.

Bové, J.M. 2006. "Huanglongbing: A Destructive, Newly-Emerging, Century-Old Disease of Citrus." *Journal of Plant Pathology* 88 (1): 7–37.

Cardinali, Marcelo Camponez do Brasil, Paulino Ribeiro Villas Boas, Débora Marcondes Bastos Pereira Milori, Ednaldo José Ferreira, Marina França e Silva, Marcos Antonio Machado, Barbara Sayuri Bellete, and Maria Fatima das Graças Fernandes da Silva. 2012. "Infrared Spectroscopy: A Potential Tool in Huanglongbing and Citrus Variegated Chlorosis Diagnosis." *Talanta* 91 (March):1–6. https://doi.org/10.1016/j.talanta.2012.01.008.

"Case History: Hyperspectral Sorting Detects More." 2021. Food Processing. June 7, 2021. https://www.foodprocessing.com/manufacturing-equipment/inspection-and-sorting/article/11298304/case-history-hyperspectral-sorting-detects-more.

Cho, Byoung-Kwan, Moon S. Kim, In-Suck Baek, Dae-Yong Kim, Wang-Hee Lee, Jongkee Kim, Hanhong Bae, and Young-Sik Kim. 2013. "Detection of Cuticle Defects on Cherry Tomatoes Using Hyperspectral Fluorescence Imagery." *Postharvest Biology and Technology* 76 (February):40–49. https://doi.org/10.1016/j.postharvbio.2012.09.002.

"Citrus Quarantine and Disease Detection Maps." 2024. Florida Department of Agriculture and Consumer Services. March 27, 2024. https://www.fdacs.gov/Agriculture-Industry/Pests-and-Diseases/Plant-Pests-and-Diseases/Citrus-Health-Response-Program/Citrus-Quarantine-and-Disease-Detection-Maps.

Cruz, J., C. D. Court, and J.P. Ferreira. 2023. "2020-2021 Economic Contributions of the Florida Citrus Industry." UF/IFAS Economic Impact Analysis Program, Food and Resource Economics Department, University of Florida. https://fred.ifas.ufl.edu/extension/economic-impact-analysis-program/publications/2020-21-citrus-economic-contributions-report/.

Dananjayan, Sathian, Yu Tang, Jiajun Zhuang, Chaojun Hou, and Shaoming Luo. 2022. "Assessment of State-of-the-Art

Deep Learning Based Citrus Disease Detection Techniques Using Annotated Optical Leaf Images." *Computers and Electronics in Agriculture* 193 (February):106658. https://doi.org/10.1016/j.compag.2021.106658.

Deng, Xiaoling, Zixiao Huang, Zheng Zheng, Yubin Lan, and Fen Dai. 2019. "Field Detection and Classification of Citrus Huanglongbing Based on Hyperspectral Reflectance." *Computers and Electronics in Agriculture* 167 (December):105006. https://doi.org/10.1016/j.compag.2019.105006.

Dewdney, Megan M., and Evan G. Johnson. 2023. "Florida Citrus Production Guide: Citrus Canker: CPG Ch. 30, CG040/PP-182, Rev. 6/2023." *EDIS*, August. https://doi.org/10.32473/edis-cg040-2023.

Dewdney, Megan M., Tripti Vashisth, and Lauren M. Diepenbrock. 2023. "Florida Citrus Production Guide: Huanglongbing (Citrus Greening): CPG Ch. 29, CG086/PP-225, Rev. 6/2023." *EDIS*, August. https://doi.org/10.32473/edis-cg086-2023.

Diezma, Belén, Lourdes Lleó, Jean Michel Roger, Ana Herrero-Langreo, Loredana Lunadei, and Margarita Ruiz-Altisent. 2013. "Examination of the Quality of Spinach Leaves Using Hyperspectral Imaging." *Postharvest Biology and Technology* 85 (November):8–17. https://doi.org/10.1016/j.postharvbio.2013.04.017.

Du, Qian, and He Yang. 2008. "Similarity-Based Unsupervised Band Selection for Hyperspectral Image Analysis." *IEEE Geoscience and Remote Sensing Letters* 5 (4): 564–68. https://doi.org/10.1109/LGRS.2008.2000619.

Duarte, André, Nuno Borralho, Pedro Cabral, and Mário Caetano. 2022. "Recent Advances in Forest Insect Pests and Diseases Monitoring Using UAV-Based Data: A Systematic Review." *Forests* 13 (6): 911. https://doi.org/10.3390/f13060911.

Frederick, Quentin, T. F. Burks, Pappu Yadav, Jianwei Qin, Moon Kim, and Megan M. Dewdney. 2024. "Classifying Adaxial and Abaxial Sides of Diseased Citrus Leaves with Selected Hyperspectral Bands and YOLOv8 | SPIE Defense + Commercial Sensing." In *Autonomous Air and Ground Sensing Systems for Agricultural Optimization and Phenotyping IX*. National Harbor, Maryland. https://spie.org/defense-commercial-sensing/presentation/Multiclass-citrus-leaf-disease-inspection-with-hyperspectral-imagery-and-custom/13053-18.

Frederick, Quentin, Pappu Yadav, Thomas Burks, Jianwei Qin, Moon Kim, and Mark Ritenour. 2023. "Selecting Hyperspectral Bands And Extracting Features With A Custom Shallow Convolutional Neural Network To Classify Citrus Peel Defects." Presented at the AI in Agriculture: Innovation and Discovery to Equitably meet Producer Needs and Perceptions, Orlando, FL, USA, April 19.

Gómez-Flores, Wilfrido, Juan José Garza-Saldaña, and Sóstenes Edmundo Varela-Fuentes. 2019. "Detection of Huanglongbing Disease Based on Intensity-Invariant Texture Analysis of Images in the Visible Spectrum." *Computers and Electronics in Agriculture* 162 (July):825–35. https://doi.org/10.1016/j.compag.2019.05.032.

Gottwald, T. R., J. H. Graham, and T. S. Schubert. 2002. "Citrus Canker: The Pathogen and Its Impact." *Plant Health Progress* 10 (1). http://dx.doi.org/10.1094/PHP-2002-0812-01-RV.

Gurubelli, Yogeswararao, R. Malmathanraj, and P. Palanisamy. 2020. "Texture and Colour Gradient Features for Grade Analysis of Pomegranate and Mango Fruits Using Kernel-SVM Classifiers." In *2020 6th International Conference on Advanced Computing and Communication Systems (ICACCS)*, 122–26. https://doi.org/10.1109/ICACCS48705.2020.9074221.

Haralick, Robert M., K. Shanmugam, and Its'Hak Dinstein. 1973. "Textural Features for Image Classification." *IEEE Transactions on Systems, Man, and Cybernetics* SMC-3 (6): 610–21. https://doi.org/10.1109/TSMC.1973.4309314.

Hogan, Hank. 2021. "The Food Industry's Appetite for Hyperspectral Imaging Grows." Photonics Media. 2021. https://www.photonics.com/Articles/The_Food_Industrys_Appetite_for_Hyperspectral/a66946.

Huang, Feng-Hua, Yan-Hong Liu, XinYi Sun, and Hua Yang. 2021. "Quality Inspection of Nectarine Based on Hyperspectral Imaging Technology." *Systems Science & Control Engineering* 9 (1): 350–57. https://doi.org/10.1080/21642583.2021.1907260.

Islam, Ashraful, Syeda Rafiatus Sama Raisa, and Nahiyan Habib Khan. 2023. "Enhanced Leafy Vegetable Analysis: Image Classification and Disease Instance Segmentation Using Deep Learning Techniques." SSRN Scholarly Paper. Rochester, NY. https://doi.org/10.2139/ssrn.4470131.

Jocher, Glenn, Ayush Chaurasia, and Jing Qiu. (2022) 2023. "Ultralytics YOLOv8." Python. Ultralytics. https://github.com/ultralytics/ultralytics.

Kukreja, Vinay, Rishabh Sharma, and Rishika Yadav. 2023. "Improving Citrus Farming Through Efficient and Accurate Diagnosis of Lemon Citrus Canker Disease with Deep Learning." In *2023 4th International Conference for Emerging Technology (INCET)*, 1–5. https://doi.org/10.1109/INCET57972.2023.10170174.

Kwak, Dong-Hoon, Guk-Jin Son, Mi-Kyung Park, and Young-Duk Kim. 2021. “Rapid Foreign Object Detection System on Seaweed Using VNIR Hyperspectral Imaging.” *Sensors* 21 (16): 5279. https://doi.org/10.3390/s21165279.

Li, Jiming, and Yuntao Qian. 2011. “Dimension Reduction of Hyperspectral Images with Sparse Linear Discriminant Analysis.” In *2011 IEEE International Geoscience and Remote Sensing Symposium*, 2927–30. https://doi.org/10.1109/IGARSS.2011.6049828.

Li, Rujia, Yadong Li, Weibo Qin, Arzlan Abbas, Shuang Li, Rongbiao Ji, Yehui Wu, Yiting He, and Jianping Yang. 2024. “Lightweight Network for Corn Leaf Disease Identification Based on Improved YOLO V8s.” *Agriculture* 14 (2): 220. https://doi.org/10.3390/agriculture14020220.

Li, Shutao, Weiwei Song, Leyuan Fang, Yushi Chen, Pedram Ghamisi, and Jon Atli Benediktsson. 2019. “Deep Learning for Hyperspectral Image Classification: An Overview.” *IEEE Transactions on Geoscience and Remote Sensing* 57 (9): 6690–6709. https://doi.org/10.1109/TGRS.2019.2907932.

Liu, Qiang, Dandan Zhou, Siying Tu, Hui Xiao, Bin Zhang, Ye Sun, Leiqing Pan, and Kang Tu. 2020. “Quantitative Visualization of Fungal Contamination in Peach Fruit Using Hyperspectral Imaging.” *Food Analytical Methods* 13 (6): 1262–70. https://doi.org/10.1007/s12161-020-01747-x.

Lu, Jianqiang, Yubin Lan, Wadi Chen, Xiaofang Qiu, Jiewei Huang, and Haoxuan Luo. 2023. “Design of Citrus Peel Defect and Fruit Morphology Detection Method Based on Machine Vision.” SSRN Scholarly Paper. Rochester, NY. https://doi.org/10.2139/ssrn.4632189.

Luo, Dehuan, Yueju Xue, Xinru Deng, Bin Yang, Haifei Chen, and Zhujiang Mo. 2023. “Citrus Diseases and Pests Detection Model Based on Self-Attention YOLOV8.” *IEEE Access* 11:139872–81. https://doi.org/10.1109/ACCESS.2023.3340148.

Lyu, Shilei, Xu Zhou, Zhen Li, Xueya Liu, Yicong Chen, and Weibin Zeng. 2023. “YOLO-SCL: A Lightweight Detection Model for Citrus Psyllid Based on Spatial Channel Interaction.” *Frontiers in Plant Science* 14 (October). https://doi.org/10.3389/fpls.2023.1276833.

Neves, Ruan F. O., Caio B. Wetterich, Elaine P. M. Sousa, and Luis G. Marcassa. 2023. “Multiclass Classifier Based on Deep Learning for Detection of Citrus Disease Using Fluorescence Imaging Spectroscopy.” *Laser Physics* 33 (5): 055602. https://doi.org/10.1088/1555-6611/acc6bd.

Ngugi, Lawrence C., Moataz Abelwahab, and Mohammed Abo-Zahhad. 2021. “Recent Advances in Image Processing Techniques for Automated Leaf Pest and Disease Recognition – A Review.” *Information Processing in Agriculture* 8 (1): 27–51. https://doi.org/10.1016/j.inpa.2020.04.004.

Nguyen, Canh, Vasit Sagan, Matthew Maimaitiyiming, Maitiniyazi Maimaitijiang, Sourav Bhadra, and Misha T. Kwasniewski. 2021. “Early Detection of Plant Viral Disease Using Hyperspectral Imaging and Deep Learning.” *Sensors* 21 (3): 742. https://doi.org/10.3390/s21030742.

Okere, Emmanuel Ekene, Alemayehu Ambaw, Willem Jacobus Perold, and Umezuruike Linus Opara. 2023. “Vis-NIR and SWIR Hyperspectral Imaging Method to Detect Bruises in Pomegranate Fruit.” *Frontiers in Plant Science* 14 (April). https://doi.org/10.3389/fpls.2023.1151697.

Olaniyi, Ebenezer O., Adefemi A. Adekunle, Temitope Odekuoye, and Adnan Khashman. 2017. “Automatic System for Grading Banana Using GLCM Texture Feature Extraction and Neural Network Arbitrations.” *Journal of Food Process Engineering* 40 (6): e12575. https://doi.org/10.1111/jfpe.12575.

Pydipati, R., T. F. Burks, and W. S. Lee. 2006. “Identification of Citrus Disease Using Color Texture Features and Discriminant Analysis.” *Computers and Electronics in Agriculture* 52 (1): 49–59. https://doi.org/10.1016/j.compag.2006.01.004.

Qiu, Rong-Zhou, Shao-Ping Chen, Mei-Xiang Chi, Rong-Bo Wang, Ting Huang, Guo-Cheng Fan, Jian Zhao, and Qi-Yong Weng. 2022. “An Automatic Identification System for Citrus Greening Disease (Huanglongbing) Using a YOLO Convolutional Neural Network.” *Frontiers in Plant Science* 13 (December). https://doi.org/10.3389/fpls.2022.1002606.

Rogers, Mitchell, Jacques Blanc-Talon, Martin Urschler, and Patrice Delmas. 2023. “Wavelength and Texture Feature Selection for Hyperspectral Imaging: A Systematic Literature Review.” *Journal of Food Measurement and Characterization* 17 (6): 6039–64. https://doi.org/10.1007/s11694-023-02044-x.

Schumann, Arnold W., Ariel Singerman, Mark A. Ritenour, Jawwad Qureshi, and Fernando Alferez. 2023. “Florida Citrus Production Guide: Citrus under Protective Screen (CUPS) Production Systems: CPG Ch. 21, HS1304/CMG19, Rev. 5/2023.” *EDIS*, August. https://doi.org/10.32473/edis-hs1304-2023.

Shuaibu, Mubarakat, Won Suk Lee, John Schueller, Paul Gader, Young Ki Hong, and Sangcheol Kim. 2018. “Unsupervised Hyperspectral Band Selection for Apple Marssonina Blotch Detection.” *Computers and Electronics in Agriculture* 148 (May):45–53. https://doi.org/10.1016/j.compag.2017.09.038.

Singerman, Ariel, and Marina Burani Arouca. 2017. “Evolution of Citrus Disease Management Programs and Their Economic Implications: The Case of Florida’s Citrus Industry.” *EDIS* 2017 (1). https://doi.org/10.32473/edis-fe915-2017.

Solawetz, Jacob, and Francesco. 2023. “What Is YOLOv8? The Ultimate Guide. [2024].” Roboflow Blog. January 11, 2023. https://blog.roboflow.com/whats-new-in-yolov8/.

Thien Pham, Quoc, and Nai-Shang Liou. 2022. “The Development of On-Line Surface Defect Detection System for Jujubes Based on Hyperspectral Images.” *Computers and Electronics in Agriculture* 194 (March):106743. https://doi.org/10.1016/j.compag.2022.106743.

Tormala, Minna, and Vittorio Calbucci. 2023. “Hyperspectral Imaging Boosts Yields in Vertical Farming.” Photonics Media. July 2023. https://www.photonics.com/Articles/Hyperspectral_Imaging_Boosts_Yields_in_Vertical/a69088.

Trinh, Dong Cong, Anh Tuan Mac, Khanh Giap Dang, Huong Thanh Nguyen, Hoc Thai Nguyen, and Thanh Dang Bui. 2024. “Alpha-EIOU-YOLOv8: An Improved Algorithm for Rice Leaf Disease Detection.” *AgriEngineering* 6 (1): 302–17. https://doi.org/10.3390/agriengineering6010018.

Velásquez, Carlos, Flavio Prieto, Lluís Palou, Sergio Cubero, José Blasco, and Nuria Aleixos. 2024. “New Model for the Automatic Detection of Anthracnose in Mango Fruits Based on Vis/NIR Hyperspectral Imaging and Discriminant Analysis.” *Journal of Food Measurement and Characterization* 18 (1): 560–70. https://doi.org/10.1007/s11694-023-02173-3.

Wang, Nian, Elizabeth A. Pierson, João Carlos Setubal, Jin Xu, Julien G. Levy, Yunzeng Zhang, Jinyun Li, Luiz Thiberio Rangel, and Joaquim Martins Jr. 2017. “The Candidatus Liberibacter–Host Interface: Insights into Pathogenesis Mechanisms and Disease Control.” *Annual Review of Phytopathology* 55 (Volume 55, 2017): 451–82. https://doi.org/10.1146/annurev-phyto-080516-035513.

Weber, Catharine, Skyler Simnitt, Helen Wakefield, Seth Wechsler, and Bryn Swearingen. 2024. “Fruit and Tree Nuts Outlook: March 2024.” Situation and Outlook FTS-378. United States Department of Agriculture. https://www.ers.usda.gov/webdocs/outlooks/108881/fts-378.pdf?v=1518.7.

Wetterich, Caio Bruno, Ruan Felipe de Oliveira Neves, José Belasque, and Luis Gustavo Marcassa. 2016. “Detection of Citrus Canker and Huanglongbing Using Fluorescence Imaging Spectroscopy and Support Vector Machine Technique.” *Applied Optics* 55 (2): 400–407. https://doi.org/10.1364/AO.55.000400.

Yang, Ce, Won Suk Lee, and Paul Gader. 2014. “Hyperspectral Band Selection for Detecting Different Blueberry Fruit Maturity Stages.” *Computers and Electronics in Agriculture* 109 (November):23–31. https://doi.org/10.1016/j.compag.2014.08.009.

Yogeshwari, M., and G. Thailambal. 2023. “Automatic Feature Extraction and Detection of Plant Leaf Disease Using GLCM Features and Convolutional Neural Networks.” *Materials Today: Proceedings*, International Virtual Conference on Sustainable Materials (IVCSM-2k20), 81 (January):530–36. https://doi.org/10.1016/j.matpr.2021.03.700.

Yuan, Deshuai, Jinbao Jiang, Xiaotong Qi, Zilin Xie, and Guangmei Zhang. 2020. “Selecting Key Wavelengths of Hyperspectral Imagine for Nondestructive Classification of Moldy Peanuts Using Ensemble Classifier.” *Infrared Physics & Technology* 111 (December):103518. https://doi.org/10.1016/j.infrared.2020.103518.

Zhang, Hailiang, Ying Chen, Xuemei Liu, Yifeng Huang, Baishao Zhan, and Wei Luo. 2021. “Identification of Common Skin Defects and Classification of Early Decayed Citrus Using Hyperspectral Imaging Technique.” *Food Analytical Methods* 14 (6): 1176–93. https://doi.org/10.1007/s12161-020-01960-8.

Zhang, Lefei, Qian Zhang, Bo Du, Xin Huang, Yuan Yan Tang, and Dacheng Tao. 2018. “Simultaneous Spectral-Spatial Feature Selection and Extraction for Hyperspectral Images.” *IEEE Transactions on Cybernetics* 48 (1): 16–28. https://doi.org/10.1109/TCYB.2016.2605044.